arXiv:1601.06590v2 [astro-ph.HE] 16 Feb 2016

Limits to dark matter annihilation cross-section from a combined analysis of MAGIC and Fermi-LAT observations of dwarf satellite galaxies

M. L. Ahnen[1] S. Ansoldi[2] L. A. Antonelli[3] P. Antoranz[4] A. Babic[5]
B. Banerjee[6] P. Bangale[7] U. Barres de Almeida[7,25] J. A. Barrio[8]
J. Becerra González[9,26] W. Bednarek[10] E. Bernardini[11,27]
B. Biasuzzi[2] A. Biland[1] O. Blanch[12] S. Bonnefoy[8] G. Bonnoli[3]
F. Borracci[7] T. Bretz[13,28] E. Carmona[14] A. Carosi[3] A. Chatterjee[6]
R. Clavero[9] P. Colin[7] E. Colombo[9] J. L. Contreras[8] J. Cortina[12]
S. Covino[3] P. Da Vela[4] F. Dazzi[7] A. De Angelis[15] B. De Lotto[2]
E. de Oña Wilhelmi[16] C. Delgado Mendez[14] F. Di Pierro[3]
D. Dominis Prester[5] D. Dorner[13] M. Doro[15] S. Einecke[17]
D. Eisenacher Glawion[13] D. Elsaesser[13] A. Fernández-Barral[12]
D. Fidalgo[8] M. V. Fonseca[8] L. Font[18] K. Frantzen[17] C. Fruck[7]
D. Galindo[19] R. J. García López[9] M. Garczarczyk[11] D. Garrido
Terrats[18] M. Gaug[18] P. Giammaria[3] N. Godinović[5] A. González
Muñoz[12] D. Guberman[12] A. Hahn[7] Y. Hanabata[20] M. Hayashida[20]
J. Herrera[9] J. Hose[7] D. Hrupec[5] G. Hughes[1] W. Idec[10]
K. Kodani[20] Y. Konno[20] H. Kubo[20] J. Kushida[20] A. La Barbera[3]
D. Lelas[5] E. Lindfors[21] S. Lombardi[3] F. Longo[2] M. López[8]
R. López-Coto[12] A. López-Oramas[12,29] E. Lorenz[7] P. Majumdar[6]
M. Makariev[22] K. Mallot[11] G. Maneva[22] M. Manganaro[9]
K. Mannheim[13] L. Maraschi[3] B. Marcote[19] M. Mariotti[15]
M. Martínez[12] D. Mazin[7,30] U. Menzel[7] J. M. Miranda[4]
R. Mirzoyan[7] A. Moralejo[12] E. Moretti[7] D. Nakajima[20]
V. Neustroev[21] A. Niedzwiecki[10] M. Nievas Rosillo[8] K. Nilsson[21,31]
K. Nishijima[20] K. Noda[7] R. Orito[20] A. Overkemping[17] S. Paiano[15]
J. Palacio[12] M. Palatiello[2] D. Paneque[7] R. Paoletti[4]
J. M. Paredes[19] X. Paredes-Fortuny[19] M. Persic[2,32] J. Poutanen[21]
P. G. Prada Moroni[23] E. Prandini[1,33] I. Puljak[5] W. Rhode[17]

M. Ribó[19] **J. Rico**[12,*] **J. Rodriguez Garcia**[7] **T. Saito**[20] **K. Satalecka**[8]
C. Schultz[15] **T. Schweizer**[7] **S. N. Shore**[23] **A. Sillanpää**[21] **J. Sitarek**[10]
I. Snidaric[5] **D. Sobczynska**[10] **A. Stamerra**[3] **T. Steinbring**[13]
M. Strzys[7] **L. Takalo**[21] **H. Takami**[20] **F. Tavecchio**[3] **P. Temnikov**[22]
T. Terzić[5] **D. Tescaro**[9] **M. Teshima**[7,30] **J. Thaele**[17] **D. F. Torres**[24]
T. Toyama[7] **A. Treves**[2] **V. Verguilov**[22] **I. Vovk**[7] **J. E. Ward**[12]
M. Will[9] **M. H. Wu**[16] **R. Zanin**[19] **(the MAGIC Collaboration)**
J. Aleksić[12,*] **M. Wood**[34,*] **B. Anderson**[35,36] **E. D. Bloom**[34]
J. Cohen-Tanugi[37] **A. Drlica-Wagner**[38] **M. N. Mazziotta**[39]
M. Sánchez-Conde[35,36] **L. Strigari**[40]

[1]ETH Zurich, CH-8093 Zurich, Switzerland

[2]Università di Udine, and INFN Trieste, I-33100 Udine, Italy

[3]INAF National Institute for Astrophysics, I-00136 Rome, Italy

[4]Università di Siena, and INFN Pisa, I-53100 Siena, Italy

[5]Croatian MAGIC Consortium, Rudjer Boskovic Institute, University of Rijeka, University of Split and University of Zagreb, Croatia

[6]Saha Institute of Nuclear Physics, 1/AF Bidhannagar, Salt Lake, Sector-1, Kolkata 700064, India

[7]Max-Planck-Institut für Physik, D-80805 München, Germany

[8]Universidad Complutense, E-28040 Madrid, Spain

[9]Inst. de Astrofísica de Canarias, E-38200 La Laguna, Tenerife, Spain; Universidad de La Laguna, Dpto. Astrofísica, E-38206 La Laguna, Tenerife, Spain

[10]University of Łódź, PL-90236 Lodz, Poland

[11]Deutsches Elektronen-Synchrotron (DESY), D-15738 Zeuthen, Germany

[12]Institut de Fisica d'Altes Energies (IFAE), The Barcelona Institute of Science and Technology, Campus UAB, 08193 Bellaterra (Barcelona), Spain

[13]Universität Würzburg, D-97074 Würzburg, Germany

[14]Centro de Investigaciones Energéticas, Medioambientales y Tecnológicas, E-28040 Madrid, Spain

[15]Università di Padova and INFN, I-35131 Padova, Italy

[16]Institute for Space Sciences (CSIC/IEEC), E-08193 Barcelona, Spain

[17]Technische Universität Dortmund, D-44221 Dortmund, Germany

[18]Unitat de Física de les Radiacions, Departament de Física, and CERES-IEEC, Universitat Autònoma de Barcelona, E-08193 Bellaterra, Spain

[19]Universitat de Barcelona, ICC, IEEC-UB, E-08028 Barcelona, Spain

[20]Japanese MAGIC Consortium, ICRR, The University of Tokyo, Department of Physics and Hakubi Center, Kyoto University, Tokai University, The University of Tokushima, KEK, Japan

[21]Finnish MAGIC Consortium, Tuorla Observatory, University of Turku and Department of Physics, University of Oulu, Finland

[22]Inst. for Nucl. Research and Nucl. Energy, BG-1784 Sofia, Bulgaria

---

*Corresponding author.

[23]Università di Pisa, and INFN Pisa, I-56126 Pisa, Italy

[24]ICREA and Institute for Space Sciences (CSIC/IEEC), E-08193 Barcelona, Spain

[25]now at Centro Brasileiro de Pesquisas Físicas (CBPF/MCTI), R. Dr. Xavier Sigaud, 150 - Urca, Rio de Janeiro - RJ, 22290-180, Brazil

[26]now at NASA Goddard Space Flight Center, Greenbelt, MD 20771, USA and Department of Physics and Department of Astronomy, University of Maryland, College Park, MD 20742, USA

[27]Humboldt University of Berlin, Institut für Physik Newtonstr. 15, 12489 Berlin Germany

[28]now at Ecole polytechnique fédérale de Lausanne (EPFL), Lausanne, Switzerland

[29]now at Laboratoire AIM, Service d'Astrophysique, DSM/IRFU, CEA/Saclay FR-91191 Gif-sur-Yvette Cedex, France

[30]also at Japanese MAGIC Consortium

[31]now at Finnish Centre for Astronomy with ESO (FINCA), Turku, Finland

[32]also at INAF-Trieste

[33]also at ISDC - Science Data Center for Astrophysics, 1290, Versoix (Geneva)

[34]W. W. Hansen Experimental Physics Laboratory, Kavli Institute for Particle Astrophysics and Cosmology, Department of Physics and SLAC National Accelerator Laboratory, Stanford University, Stanford, CA 94305, USA

[35]Department of Physics, Stockholm University, AlbaNova, SE-106 91 Stockholm, Sweden

[36]The Oskar Klein Centre for Cosmoparticle Physics, AlbaNova, SE-106 91 Stockholm, Sweden

[37]Laboratoire Univers et Particules de Montpellier, Université Montpellier, CNRS/IN2P3, Montpellier, France

[38]Center for Particle Astrophysics, Fermi National Accelerator Laboratory, Batavia, IL 60510, USA

[39]Istituto Nazionale di Fisica Nucleare, Sezione di Bari, I-70126 Bari, Italy

[40]Texas A&M University, Department of Physics and Astronomy, College Station, TX 77843-4242, USA

E-mail: jrico@ifae.es, mdwood@slac.stanford.edu, jelena@ifae.es

Abstract.

We present the first joint analysis of gamma-ray data from the MAGIC Cherenkov telescopes and the *Fermi* Large Area Telescope (LAT) to search for gamma-ray signals from dark matter annihilation in dwarf satellite galaxies. We combine 158 hours of Segue 1 observations with MAGIC with 6-year observations of 15 dwarf satellite galaxies by the *Fermi*-LAT. We obtain limits on the annihilation cross-section for dark matter particle masses between 10 GeV and 100 TeV – the widest mass range ever explored by a single gamma-ray analysis. These limits improve on previously published *Fermi*-LAT and MAGIC results by up to a factor of two at certain masses. Our new inclusive analysis approach is completely generic and can be used to perform a global, sensitivity-optimized dark matter search by combining data from present and future gamma-ray and neutrino detectors.

Keywords: dark matter experiments, gamma ray experiments, neutrino experiments, dwarf galaxies

Contents

1   Introduction

The existence of a non-baryonic, neutral and cold dark matter (DM) component in the Universe is supported by an overwhelming body of observational evidence, mainly involving its gravitational effects on the dynamics of cosmic structures like galaxy clusters (first observed by Zwicky in 1933 [1]) and spiral galaxies [2, 3], and on the power spectrum of temperature anisotropies of the cosmic microwave background [4, 5]. Several theories beyond the Standard Model postulate the existence of a new neutral, stable and weakly interacting massive particle (generically known as WIMP [6]), with mass in the TeV scale, and that could account for the measured DM relic density (e.g. [7]).

A promising way to identify the nature of DM and to measure its properties is to search for the Standard Model (SM) particles produced through WIMP annihilation or decay at DM over-densities, or *halos*, in the local Universe. Among those SM products, gamma rays and neutrinos are the only stable neutral particles. They travel from their production sites to Earth unaffected by magnetic deflection, and as such are ideal messengers for astronomical DM searches.

Current gamma-ray instruments like the *Fermi* Large Area Telescope (LAT)[1] in space, the ground-based Cherenkov telescopes MAGIC[2], H.E.S.S.[3] and VERITAS[4], the new-generation water Cherenkov detector HAWC[5], as well as neutrino telescopes like Antares[6], IceCube[7], and SuperKamiokande[8], are sensitive to overlapping and/or complementary DM particle mass ranges (from ∼1 GeV to ∼100 TeV). All these instruments have dedicated programs

---

[1]http://fermi.gsfc.nasa.gov
[2]http://magic.mpp.mpg.de
[3]http://www.mpi-hd.mpg.de/hfm/HESS
[4]http://veritas.sao.arizona.edu
[5]http://www.hawc-observatory.org
[6]http://antares.in2p3.fr
[7]http://icecube.wisc.edu
[8]http://www-sk.icrr.u-tokyo.ac.jp/sk/index-e.html

to look for WIMP signals coming from, e.g., the Galactic Center and halo [8–17], galaxy clusters [18–22], dwarf spheroidal galaxies (dSphs) [23–34] and other targets [35–37].

A natural step forward within this collective effort is the combination of data from different experiments and/or observational targets, which allows a global and sensitivity-optimized search [38]. This can be achieved in a relatively straightforward way since, for a given DM particle model, a joint likelihood function can be written as the product of the particular likelihood functions for each of the measurements/instruments. One advantage of such an approach is that the details of each experiment, such as event lists or instrument response functions (IRFs), do not need to be combined or averaged.

In this paper, we present a new global analysis framework for DM searches, applicable to observations from gamma-ray and neutrino instruments, and the results of applying it to the MAGIC and *Fermi*-LAT observations of dSphs.

DSphs are associated with the population of Galactic DM sub-halos, predicted by the cold DM structure formation scenario and reproduced in N-body cosmological simulations (e.g. [39, 40]), that have accreted enough baryonic mass to form stars (other sub-halos may remain completely dark). DSphs have very high mass-to-light ratios, being the most DM-dominated systems known so far [41]. They have the advantage of being free of other sources of gamma-ray emission and have been identified predominantly at high Galactic latitudes, where diffuse astrophysical foregrounds from the Milky Way are lowest. Because they are relatively close, they are expected to appear as point-like or marginally extended sources for gamma-ray and neutrino telescopes, with relatively high DM annihilation fluxes. The stellar kinematics of these systems can be used to determine their DM distribution and its uncertainty using a common methodology [42–44]. These measurements enable the combination of dSph observations that constrains models of DM annihilation or decay within the dSph population as a whole.

This article is organized as follows: Section 2 describes the MAGIC and *Fermi*-LAT instruments, and the data sets used in our study. The global analysis framework is described in Section 3. The results of applying the analysis to MAGIC and *Fermi*-LAT data are presented in Section 4. Finally, in Section 5 we discuss those results and present our conclusions.

2 Instruments and Observations

2.1 The MAGIC telescopes

The *Florian Goebel* Major Atmospheric Gamma-ray Imaging Cherenkov (MAGIC) telescopes are located at the Roque de los Muchachos Observatory (28.8° N, 17.9° W; 2200 m above sea level), on the Canary Island of La Palma, Spain. MAGIC is a system of two telescopes that detect Cherenkov light produced by the atmospheric particle showers initiated by cosmic particles entering the Earth's atmosphere. Images of these showers are projected by the MAGIC reflectors onto the photo-multiplier tube (PMT) cameras, and are used to reconstruct the calorimetric and spatial properties, as well as the nature of the primary particle. Thanks to its large reflectors (17 meter diameter), plus its high-quantum-efficiency and low-noise PMTs, MAGIC achieves high sensitivity to Cherenkov light and low energy threshold [45]. The MAGIC telescopes are able to detect cosmic gamma rays in the very high energy (VHE) domain, i.e. in the range between ∼50 GeV and ∼50 TeV.

For this work we use MAGIC data corresponding to 158 hours of observations of the satellite galaxy Segue 1 [32], the deepest observations of any dSph by a Cherenkov telescope

to date.[9] The data were taken between 2011 and 2013, with observations before, during, and after a major hardware upgrade [46]. This resulted in the necessity of defining 4 different observation periods, each described by a different set of IRFs. Observations were performed in the so-called wobble mode, which allows simultaneous observations of the target and the background control regions. For that purpose, two different positions $\sim 0.4°$ away from the position of Segue 1 were tracked alternatively for 20 min runs. For each of these positions, the spectral shape of the residual background is slightly different, and needs to be modeled independently. Therefore, for MAGIC, we consider 8 independent data sets, each consisting of the gamma-ray candidate events plus the corresponding IRFs and residual background models. The MAGIC data are analyzed with a one-dimensional unbinned likelihood fit to the energy distribution within a signal (or ON) region of radius $0.122°$ around the center of Segue 1 (optimized for a source with the angular size of Segue 1). The integral of the DM emission template within the ON region defines the model for the expected signal distribution as a function of energy. See Section 3.2 and Ref. [32] for more details about the MAGIC data analysis.

2.2 The *Fermi*-LAT

The *Fermi*-LAT is a pair-conversion telescope that is sensitive to gamma rays in the energy range from 20 MeV to more than 300 GeV [47]. With its large field-of-view (2.4 sr), the LAT is able to efficiently survey the entire sky. Since its launch in June 2008, the LAT has primarily operated in a survey observation mode that continuously scans the entire sky every 3 hours. The survey-mode exposure coverage is fairly uniform with variations of at most 30% with respect to the average exposure. The LAT point-source sensitivity, which is dependent on the intensity of diffuse backgrounds, shows larger variations but is relatively constant at high Galactic latitudes ($|b| > 10°$). More details on the on-orbit performance of the LAT are provided in Ref. [48].

The *Fermi*-LAT data set used in this work corresponds to 6 years of observations of 15 dSphs. We analyzed the data with the latest (Pass 8) event-level analysis [34], using the *Fermi* Science Tools version 10-01-01 and the P8R2_SOURCE_V6 IRFs. DM signal morphological and spectral templates are used in a three-dimensional likelihood fit to the distribution of events in reconstructed energy and direction within the $10° \times 10°$ dSph region-of-interest (ROI). The model for each ROI contains the dSph DM intensity template, templates for Galactic and isotropic diffuse backgrounds, and point sources taken from the third LAT source catalog (3FGL) [49] within $15°$ of the ROI center. A broadband fit in each ROI is performed fitting the normalizations of the Galactic and isotropic diffuse components and 3FGL sources that fall within the ROI boundary. After performing the broadband fit, a set of likelihoods is extracted for each energy bin by scanning the flux normalization of a putative DM source modeled as a power law with spectral index 2 at the location of the dSph. Tables with likelihood values versus energy flux for each energy bin are produced for all considered targets. The likelihood tables used for the present work are taken from Ref. [34] and can be found in the corresponding online material.[10] These tables allow the computation of joint-likelihood values for any gamma-ray spectrum, and are used as input to the present analysis (see Section 3.2 for more details).

---

[9] Older MAGIC single-telescope DM searches (Draco [29], 7.8 hours; Willman 1 [30], 15.5 hours; and Segue 1 [31], 29.4 hours) yield a comparatively poor sensitivity [32] and are therefore not included in this work.

[10] http://www-glast.stanford.edu/pub_data/1048/.

3   Analysis

3.1   Dark Matter annihilation flux

The gamma-ray (or neutrino) flux produced by DM annihilation in a given region of the sky $(\Delta\Omega)$ and observed at Earth is given by:

$$\frac{d\Phi}{dE}(\Delta\Omega) = \frac{1}{4\pi}\frac{\langle\sigma v\rangle J(\Delta\Omega)}{2m_{\mathrm{DM}}^2}\frac{dN}{dE} \quad , \qquad (3.1)$$

where m_{DM} is the mass of the DM particle, $\langle\sigma v\rangle$ the thermally-averaged annihilation cross-section, dN/dE the average gamma-ray spectrum per annihilation reaction (for neutrinos this term includes the oscillation probability between target and Earth), and

$$J(\Delta\Omega) = \int_{\Delta\Omega} d\Omega' \int_{\mathrm{l.o.s.}} dl\,\rho^2(l,\Omega') \qquad (3.2)$$

is the so-called *astrophysical factor* (or simply the J-factor), with ρ being the DM density, and the integrals running over $\Delta\Omega$ and the line-of-sight (l.o.s.) through the DM distribution.

Using the PYTHIA simulation package version 8.205 [50], we have computed the average gamma-ray spectrum per annihilation process (dN/dE) for a set of DM particles of masses between 10 GeV and 100 TeV (i.e. in the WIMP range), annihilating into SM pairs $b\bar{b}$, W^+W^-, $\tau^+\tau^-$ and $\mu^+\mu^-$. For each channel and mass, we average the gamma-ray spectrum resulting from 10^7 decay events of a generic resonance with mass $2\times m_{\mathrm{DM}}$ into the specified pairs. For each simulated event, we trace all the decay chains, including the muon radiative decay ($\mu^- \to e^-\bar{\nu}_e\nu_\mu\gamma$, not active in PYTHIA by default), down to stable particles.

We take J-factors around the analyzed dSphs from Ackermann et al. [34], who follow the approach of Ref. [42]. The DM distributions in the halos of the dSphs are parameterized following a Navarro-Frenk-White (NFW) profile [51]:

$$\rho(r) = \frac{\rho_0 r_s^3}{r(r_s+r)^2} \quad , \qquad (3.3)$$

where r_s and ρ_0 are the NFW scale radius and characteristic density, respectively, and are determined from a fit to the dSph stellar surface density and velocity dispersion profiles. The properties of the dSphs used in our analysis, including the J-factors and their uncertainties, are summarized in Table 1. We quote the measured J-factors (J_{obs}) for a reference integrated radius of $0.5°$ from the halo center in all cases, which encompasses more than 90% of the annihilation flux for our dSph halo models (which have halo scale radii between $0.1°$ and $0.4°$). We note that Table 1 together with Equations 3.2 and 3.3 allow the computation of the J-factors for any other considered $\Delta\Omega$, and therefore the DM emission templates. In Ref. [34] it has been shown how the *Fermi*-LAT limits can vary by up to $\sim 35\%$ (for a 100 GeV DM mass, and decreasing with the mass value) by assuming different parameterizations for the DM density profile in dSphs.

Using Equation 3.1 together with the values of dN/dE and J obtained as detailed in the previous paragraphs, we compute morphological and spectral intensity templates for the DM emission in each dSph. Folding these templates with the response of the MAGIC and LAT instruments, we compute the expected count distribution as a function of the measured energy and position within the observed field of each dSph.

Name	l	b	D	r_s/D	$\log_{10}(J_{\mathrm{obs}})$
	[deg]	[deg]	[kpc]	[deg]	$[\log_{10}(\mathrm{GeV}^2\mathrm{cm}^{-5})]$
Bootes I	358.08	69.62	66	0.23	18.8 ± 0.22
Canes Venatici II	113.58	82.70	160	0.071	17.9 ± 0.25
Carina	260.11	-22.22	105	0.093	18.1 ± 0.23
Coma Berenices	241.89	83.61	44	0.23	19.0 ± 0.25
Draco	86.37	34.72	76	0.26	18.8 ± 0.16
Fornax	237.10	-65.65	147	0.17	18.2 ± 0.21
Hercules	28.73	36.87	132	0.081	18.1 ± 0.25
Leo II	220.17	67.23	233	0.071	17.6 ± 0.18
Leo IV	265.44	56.51	154	0.072	17.9 ± 0.28
Sculptor	287.53	-83.16	86	0.25	18.6 ± 0.18
Segue 1	220.48	50.43	23	0.36	19.5 ± 0.29
Sextans	243.50	42.27	86	0.13	18.4 ± 0.27
Ursa Major II	152.46	37.44	32	0.32	19.3 ± 0.28
Ursa Minor	104.97	44.80	76	0.35	18.8 ± 0.19
Willman 1	158.58	56.78	38	0.25	19.1 ± 0.31

Table 1: DSphs used in the present analysis and their main properties: Name, Galactic longitude and latitude, distance to Earth, angular size of the DM halo scale radius, and J-factor (with statistical uncertainty) assuming an NFW density profile and integrated to a radius of $0.5°$ from the dSph center.

3.2   Likelihood analysis

For each considered annihilation channel and DM particle mass, we compute the profile likelihood ratio as a function of $\langle\sigma v\rangle$ (see, e.g. [52]):

$$\lambda_P(\langle\sigma v\rangle \,|\, \boldsymbol{\mathcal{D}}) = \frac{\mathcal{L}(\langle\sigma v\rangle; \hat{\hat{\boldsymbol{\nu}}} \,|\, \boldsymbol{\mathcal{D}})}{\mathcal{L}(\widehat{\langle\sigma v\rangle}; \hat{\boldsymbol{\nu}} \,|\, \boldsymbol{\mathcal{D}})} \quad , \tag{3.4}$$

with $\boldsymbol{\mathcal{D}}$ representing the data set and $\boldsymbol{\nu}$ the nuisance parameters.[11] $\widehat{\langle\sigma v\rangle}$ and $\hat{\boldsymbol{\nu}}$ are the values maximizing the joint likelihood function ($\mathcal{L}$), and $\hat{\hat{\boldsymbol{\nu}}}$ the value that maximizes $\mathcal{L}$ for a given value of $\langle\sigma v\rangle$. The likelihood function can be written as:

$$\mathcal{L}(\langle\sigma v\rangle; \boldsymbol{\nu} \,|\, \boldsymbol{\mathcal{D}}) = \prod_{i=1}^{N_{\mathrm{target}}} \mathcal{L}_i(\langle\sigma v\rangle; J_i, \boldsymbol{\mu}_i \,|\, \boldsymbol{\mathcal{D}}_i) \cdot \mathcal{J}(J_i \,|\, J_{\mathrm{obs},i}, \sigma_i) \quad , \tag{3.5}$$

where the index i runs over the different targets (dSphs in our case); J_i is the J-factor for the corresponding target (see Equations 3.2 and 3.3); $\boldsymbol{\mu}_i$ denotes any nuisance parameters additional to J_i; and $\boldsymbol{\mathcal{D}}_i$ is the target-related input data. $\mathcal{J}$ is the likelihood for J_i, given measured $\log_{10}(J_{\mathrm{obs},i})$ and its uncertainty σ_i [34]:

$$\mathcal{J}(J_i \,|\, J_{\mathrm{obs},i}, \sigma_i) = \frac{1}{\ln(10) J_{\mathrm{obs,i}} \sqrt{2\pi}\sigma_i} \times e^{-\left(\log_{10}(J_i) - \log_{10}(J_{\mathrm{obs,i}})\right)^2 / 2\sigma_i^2} \quad . \tag{3.6}$$

---

[11]In statistics, nuisance parameters are those that are not of intrinsic interest but that must be included for an accurate description of the data.

The likelihood function for a particular target ($\mathcal{L}_i$) can in turn be written as the product of the likelihoods for different instruments (represented by the index j), i.e.:

$$\mathcal{L}_i(\langle\sigma v\rangle; J_i, \boldsymbol{\mu}_i \,|\, \boldsymbol{\mathcal{D}}_i) = \prod_{j=1}^{N_{\text{instrument}}} \mathcal{L}_{ij}(\langle\sigma v\rangle; J_i, \boldsymbol{\mu}_{ij} \,|\, \boldsymbol{\mathcal{D}}_{ij}) \quad , \tag{3.7}$$

where $\boldsymbol{\mu}_{ij}$ and $\boldsymbol{\mathcal{D}}_{ij}$ represent the nuisance parameters and input data set for the given target i and instrument j. Equations 3.4, 3.5 and 3.7 are generic, i.e. they are valid for any set of instruments and observed targets.[12]

In our case, the likelihood for a given target i observed by the *Fermi*-LAT ($j \equiv F$) is computed as:

$$\mathcal{L}_{iF}(\langle\sigma v\rangle; J_i, \hat{\boldsymbol{\mu}}_{iF} \,|\, \boldsymbol{\mathcal{D}}_{iF}) = \prod_{k=1}^{N_{\text{E-bins}}} \mathcal{L}_{iFk}\big(\overline{E\Phi}_k(\langle\sigma v\rangle, J_i)\big) \quad , \tag{3.10}$$

with k running over energy bins, and

$$\overline{E\Phi}_k(\langle\sigma v\rangle, J_i) = \int_{E_{\min,k}}^{E_{\max,k}} dE\, E\, \frac{d\Phi}{dE}(\langle\sigma v\rangle, J_i) \quad . \tag{3.11}$$

The values of $\mathcal{L}_{iFk}$ vs. $\overline{E\Phi}$ corresponding to 6 years of observations of each of the considered dSph are tabulated and released by the *Fermi*-LAT Collaboration [33, 34].

For the case of MAGIC ($j \equiv M$), the likelihood corresponding to a given target i can be written as:

$$\mathcal{L}_{iM}(\langle\sigma v\rangle; J_i, \boldsymbol{\mu}_{iM} \,|\, \boldsymbol{\mathcal{D}}_{iM}) = \prod_{k=1}^{N} \mathcal{L}_{iMk}(\langle\sigma v\rangle; J_i, \boldsymbol{\mu}_{iMk} \,|\, \boldsymbol{\mathcal{D}}_{iMk}) \quad , \tag{3.12}$$

with the index k running over $N = 8$ different data sets (each described by a different IRF, see Section 2.1). The likelihood for a given data set follows the method described in Refs. [38] and [32] and can be written as (target, experiment and data set indices are omitted for

---

[12]It is also worth noting that the values of $\mathcal{L}_{ij}$ ultimately depend on the flux of DM-induced gamma rays, hence on the product $\langle\sigma v\rangle \cdot J_i$ (see Equation 3.1). Therefore, in order to compute $\mathcal{L}_i$ and $\mathcal{L}$ (and its profile with respect to J_i) it is enough to know (in addition to $\mathcal{J}$) the values of $\mathcal{L}_{ij}$ vs. $\langle\sigma v\rangle$, for fixed values of J_i (e.g. for $J_{\text{obs},i}$), since:

$$\mathcal{L}_{ij}(\langle\sigma v\rangle; J_i, \boldsymbol{\mu}_{ij} \,|\, \boldsymbol{\mathcal{D}}_{ij}) = \mathcal{L}_{ij}\big(\frac{J_i}{J_{\text{obs},i}}\langle\sigma v\rangle, J_{\text{obs},i}, \boldsymbol{\mu}_{ij} \,|\, \boldsymbol{\mathcal{D}}_{ij}\big) \quad . \tag{3.8}$$

This is a particularly useful property, since it allows a significant reduction of the computing time requested for the profile of $\mathcal{L}$ over J_i, which can be explicitly written as:

$$\mathcal{L}(\langle\sigma v\rangle; \hat{\boldsymbol{\nu}} \,|\, \boldsymbol{\mathcal{D}}) = \prod_{i=1}^{N_{\text{target}}} \max_{J_i}\{\mathcal{L}_i(\langle\sigma v\rangle; J_i, \hat{\boldsymbol{\mu}} \,|\, \boldsymbol{\mathcal{D}}_i) \cdot \mathcal{J}(J_i \,|\, J_{\text{obs},i}, \sigma_i)\} \quad , \tag{3.9}$$

where the values of $\mathcal{L}_i$ vs. J_i can be computed using Equations 3.7 and 3.8. In addition, this allows the combination of results from different instruments and targets, starting from tabulated values of $\mathcal{L}_{ij}$ vs. $\langle\sigma v\rangle$, for a fixed value of J_i and profiled with respect to $\boldsymbol{\mu}_{ij}$. These values can be produced and shared by different experiments without the need of releasing or sharing any of the internal information used to produce them, such as event lists or IRFs.

the sake of clarity):

$$\mathcal{L}(\langle\sigma v\rangle; J, \boldsymbol{\mu} \,|\, \boldsymbol{\mathcal{D}}) = \mathcal{L}\big(g(\langle\sigma v\rangle, J,); b, \tau \,|\, \{E'_l\}_{l=1,...,N_{\text{ON}}}, \{E'_m\}_{m=1,...,N_{\text{OFF}}}\big) \qquad (3.13)$$

$$= \frac{(g + b/\tau)^{N_{\text{ON}}}}{N_{\text{ON}}!} e^{-(g+b/\tau)} \frac{b^{N_{\text{OFF}}}}{N_{\text{OFF}}!} e^{-b} \prod_{l=1}^{N_{\text{ON}}} f(g; b, \tau \,|\, E'_l) \prod_{m=1}^{N_{\text{OFF}}} h(E'_m) \quad ,$$

where g is the expected number of gamma rays detected with reconstructed energy E' in the telescope range $[E'_{\text{min}}, E'_{\text{max}}]$ and an observation time T_{obs}, i.e.:

$$g(\langle\sigma v\rangle, J) = T_{\text{obs}} \int_{E'_{\text{min}}}^{E'_{\text{max}}} dE' \int_0^{\infty} dE \frac{d\Phi}{dE}(\langle\sigma v\rangle, J) \, A(E) \, G(E; E') \quad , \qquad (3.14)$$

τ and b (nuisance parameters) are the ratio of exposures between the OFF (background control) and ON (signal) regions and the expected number of background events in the OFF region, respectively. h and f are, respectively, the probability density functions (PDFs) for measured OFF and ON events with reconstructed energy E'. h is obtained by fitting or interpolating the measured differential event rate from one or several additional background control regions observed simultaneously to the ON and OFF regions (see Ref. [53] for details). Finally, f can be written as:

$$f(g; b, \tau \,|\, E') = \frac{\frac{b}{\tau} h(E') + g \, p(E')}{\frac{b}{\tau} + g} \quad , \qquad (3.15)$$

with

$$p(E') = \frac{T_{\text{obs}} \int_0^{\infty} dE \frac{d\Phi}{dE}(\langle\sigma v\rangle, J) \, A(E) \, G(E; E')}{g} \quad . \qquad (3.16)$$

$A(E)$ is the telescope effective area computed for a gamma-ray source with the morphology expected for Segue 1 according to Equations 3.1 to 3.3, after analysis cuts (including the selection of events in the ON region with radius of 0.122° around Segue 1 center). $G(E; E')$ is the PDF for the energy estimator (E') for a given true energy (E). Note that p is also a PDF and therefore does not depend on T_{obs}, J or $\langle\sigma v\rangle$.

4 Results

We compute one-sided, 95% confidence level upper limits to $\langle\sigma v\rangle$ by numerically solving the equation $-2\ln\lambda_P(\langle\sigma v\rangle_{2.71} \,|\, \boldsymbol{\mathcal{D}}) = 2.71$, with $\langle\sigma v\rangle$ restricted to the physical (≥ 0) region. This prescription is the one used by the *Fermi*-LAT Collaboration in Refs. [33, 34], and differs slightly from the one used by MAGIC in Ref. [32]. This has consequences on the comparison of the results presented here with previous MAGIC results, which will be discussed below.

Figure 1 illustrates for an individual target how the combination of experiments improves the sensitivity to DM searches, and how the J-factor statistical uncertainties worsen it. The figure shows $-2\ln(\lambda_P)$ vs. $\langle\sigma v\rangle$ for $m_{\text{DM}} = 1\,\text{TeV}$ DM particles annihilating into $b\bar{b}$ pairs in Segue 1. MAGIC and *Fermi*-LAT individual curves are shown, as well as their combination. The effect of the statistical uncertainty on the J-factor is also illustrated by showing curves where J is treated as either a nuisance or fixed parameter. In each case, the 95% confidence level upper limits are obtained from the crossing point between the corresponding curve and the $-2\ln(\lambda_P) = 2.71$ line. In the case of treating J as a nuisance parameter, MAGIC and
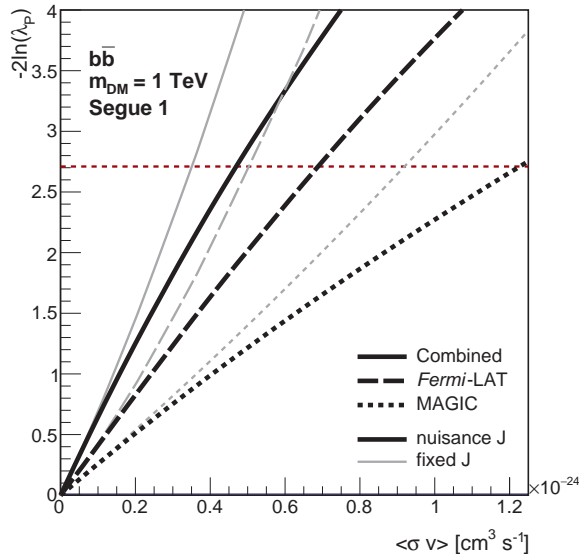
Figure 1: $-2\ln(\lambda_P)$ vs. thermally-averaged cross-section ($\langle\sigma v\rangle$) for 1 TeV DM particles annihilating into $b\bar{b}$ pairs in the Segue 1 dSph. Dotted, dashed and solid lines represent the values for MAGIC, *Fermi*-LAT, and their combination, respectively. Thick-black and thin-gray lines represent the $-2\ln(\lambda_P)$ functions when the J-factor is considered as a nuisance or fixed parameter, respectively. The horizontal dashed-red line shows the level determining, for each case, the one-sided 95% confidence level upper limits.

Fermi-LAT individual limits are $\langle\sigma v\rangle^{\mathrm{UL}} = 1.2 \times 10^{-24}$ cm^3 s^{-1} and 6.8×10^{-25} cm^3 s^{-1}, respectively, whereas the combined analysis yields $\langle\sigma v\rangle^{\mathrm{UL}} = 4.6\times10^{-25}$ cm^3 s^{-1}. Considering no uncertainties in J produces the combined limit $\langle\sigma v\rangle^{\mathrm{UL}} = 3.4 \times 10^{-25}$ cm^3 s^{-1}.

Figures 2 and 3 show our main results: the 95% confidence level limits to $\langle\sigma v\rangle$ for DM particles with masses between 10 GeV and 100 TeV annihilating into SM pairs $b\bar{b}$, W^+W^-, $\tau^+\tau^-$ and $\mu^+\mu^-$, as obtained from the combination of *Fermi*-LAT and MAGIC observations of 15 dSphs and Segue 1 alone, respectively. We also show the observed limits obtained with MAGIC and *Fermi*-LAT data considered individually. The combined limits are compared to the median, and the 68% and 95% containment bands, expected under the null ($H_0 : \langle\sigma v\rangle = 0$) hypothesis. These are estimated from the distributions of limits obtained by applying our analysis to 300 independent H_0 realizations. Each realization consists of data from *Fermi*-LAT observations of one empty field per considered dSph, combined with fast simulations of MAGIC Segue 1 observations. The empty fields constituting the LAT realizations were selected by choosing random sky positions with $|b| > 30°$ centered at least $0.5°$ away from a source in the 3FGL catalog. MAGIC fast simulations consist of a set of event energies randomly generated according to the background PDF, h (see Section 3.2 and Ref. [32] for details), for both ON and OFF regions. In all cases, we assume the same exposures on the different considered dSph as for the real data, and J-factors randomly selected according to the PDF in Equation 3.6.

We observe no evidence for DM annihilation in our data set (which would appear as a positive deviation of the limit from the null hypothesis). The maximum such deviation has a (local) significance of about $0.3\,\sigma$, found for $m_{\mathrm{DM}} \simeq 10$ GeV in the $b\bar{b}$ and $\tau^+\tau^-$ annihilation channels, and for $m_{\mathrm{DM}} \simeq 3$ TeV in the $\mu^+\mu^-$ and $\tau^+\tau^-$ annihilation channels. We also observe a negative $2\,\sigma$ fluctuation at $m_{\mathrm{DM}} \simeq 5$ TeV in the $b\bar{b}$ and W^+W^- annihilation channels and $m_{\mathrm{DM}} \simeq 500$ GeV in the $\mu^+\mu^-$ and $\tau^+\tau^-$ annihilation channels. A deviation of
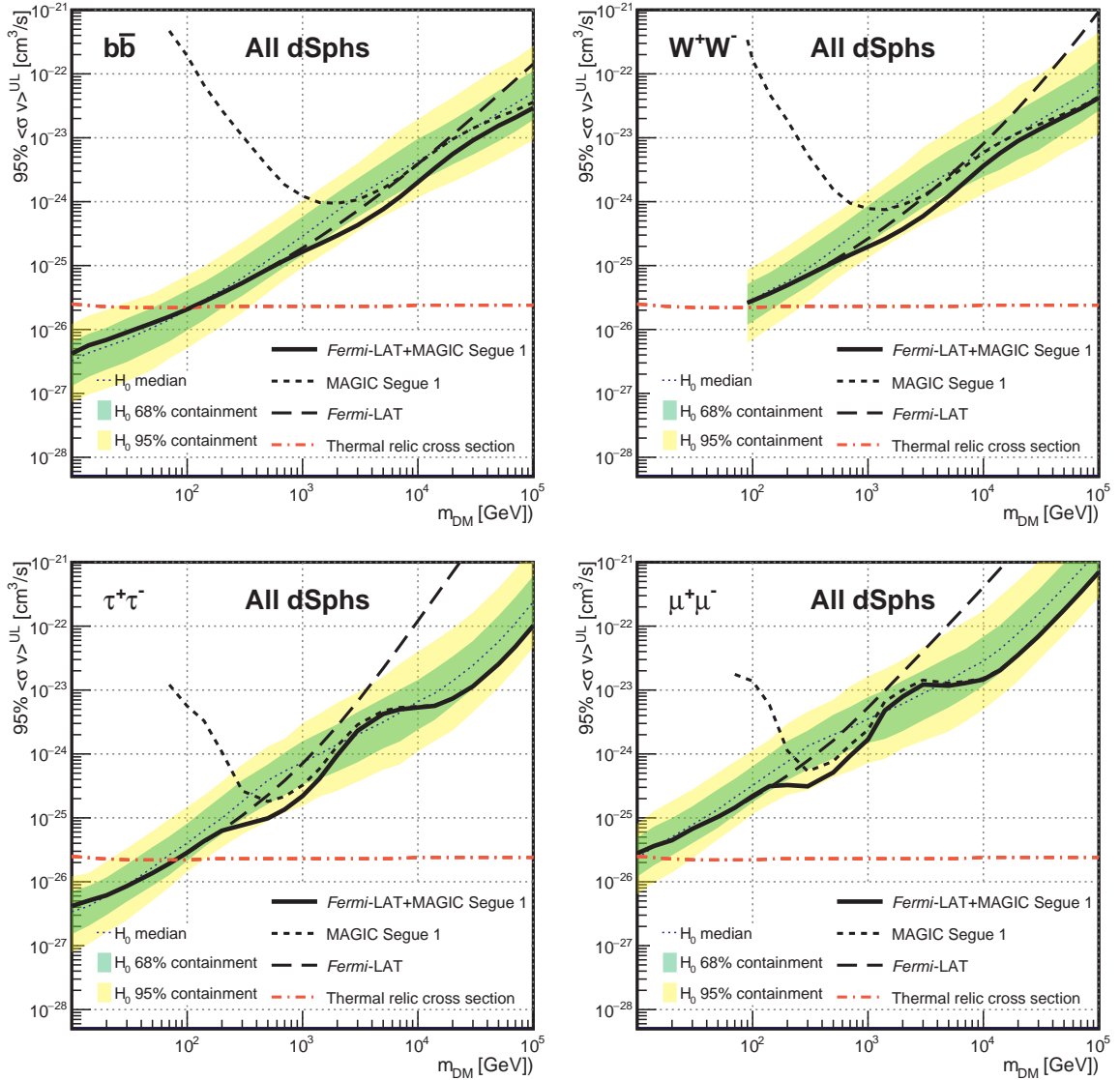
Figure 2: 95% CL upper limits on the thermally-averaged cross-section for DM particles annihilating into $b\bar{b}$ (upper-left), W^+W^- (upper-right), $\tau^+\tau^-$ (bottom-left) and $\mu^+\mu^-$ (bottom-right) pairs. Thick solid lines show the limits obtained by combining *Fermi*-LAT observations of 15 dSphs with MAGIC observations of Segue 1. Dashed lines show the observed individual MAGIC (short dashes) and *Fermi*-LAT (long dashes) limits. J-factor statistical uncertainties (Table 1) are considered as described in Section 3.2. The thin-dotted line, green and yellow bands show, respectively, the median and the symmetrical, two-sided 68% and 95% containment bands for the distribution of limits under the null hypothesis (see main text for more details). The red-dashed-dotted line shows the thermal relic cross-section from Ref. [54].

this magnitude would be expected in 5% of the experiments under the null hypothesis and is therefore compatible with random fluctuations.

As expected, limits in the low and high ends of the considered mass range are dominated by *Fermi*-LAT and MAGIC observations, respectively, and the combined limits coincide with the individual ones. The combination provides a significant improvement in the range between ~1 and ~100 TeV (for $b\bar{b}$ and W^+W^-) or ~0.2 and ~2 TeV (for $\tau^+\tau^-$ and $\mu^+\mu^-$),
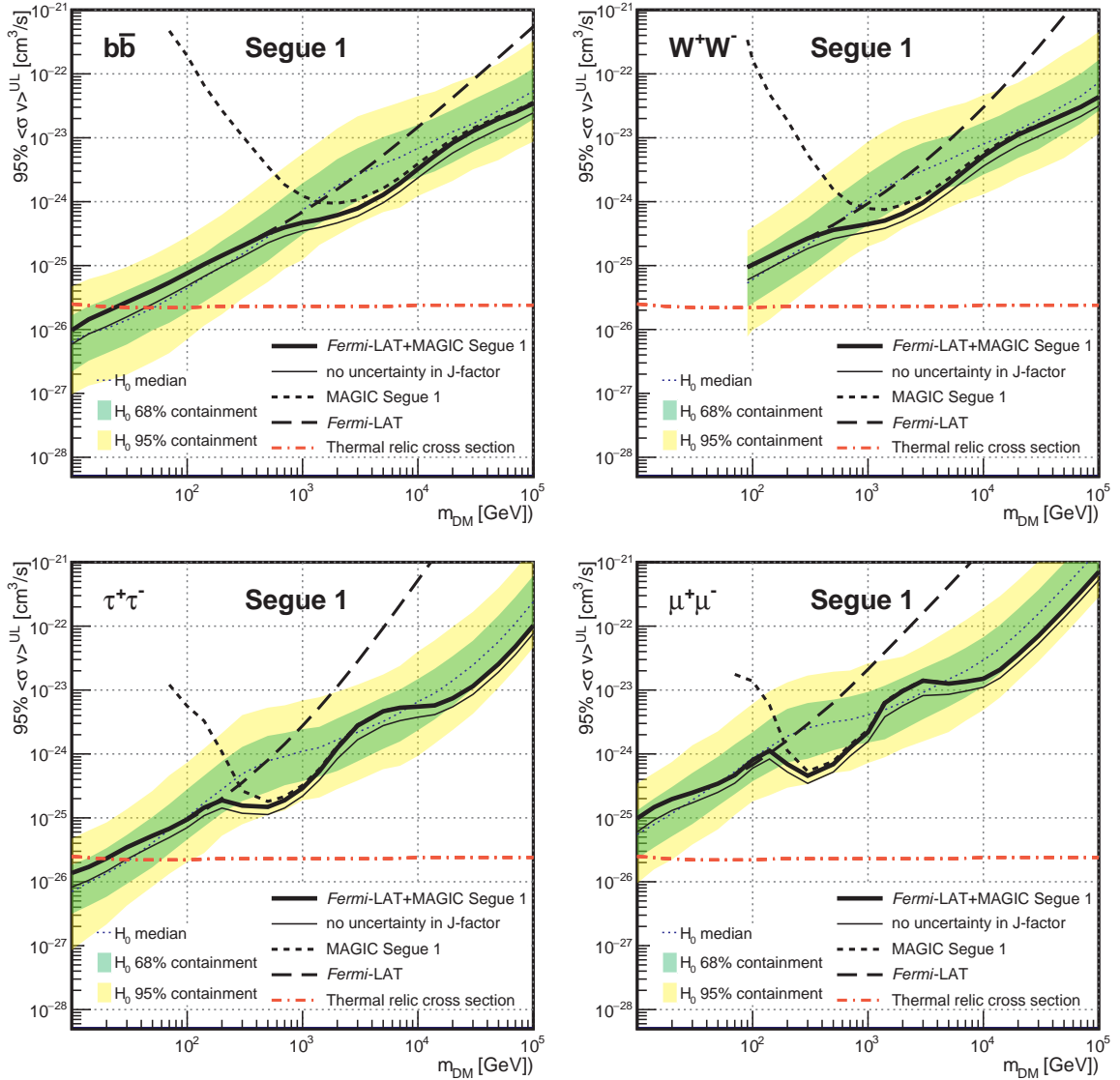
Figure 3: Similar as Figure 2 using Segue 1 observations only. The combined limits for the case when the J-factor is considered as a fixed (no statistical uncertainties) parameter are shown as a thin-solid line.

with a maximum improvement of the combined limits with respect to the individual ones by a factor ∼2. MAGIC individual limits shown in this work are stronger by up to a factor ∼4 than those presented in Ref. [32], which needs a dedicated explanation, provided in Appendix A.

Systematic uncertainties in the determination of the J-factors would weaken the limits on ⟨σv⟩ that can be inferred from the MAGIC and *Fermi*-LAT observations. In this work we take the J-factors and associated uncertainties from Ref. [42], which are largely consistent with the independent analysis of Ref. [43]. The analysis presented in Ref. [44], using a more flexible parameterization for the stellar velocity distributions and more stringent criteria for stellar membership, produces substantially larger J-factor uncertainties for the ultra-faint dSphs used in the present study (0.4–2.0 dex versus 0.2–0.3 dex). They find the J-

factor of Segue 1 to be particularly uncertain due to the ambiguous membership status of a few stars, and when excluding stars with membership probability less than 95% they find $\log_{10}(J_{\rm obs}/({\rm GeV^2\ cm^{-5}})) = 17.0^{+2.1}_{-2.2}$. This value is more than two orders of magnitude smaller than the J-factor used in the present analysis ($\log_{10}(J_{\rm obs}/({\rm GeV^2\ cm^{-5}})) = 19.5 \pm 0.3$) and would imply substantially weaker limits from the MAGIC observations of Segue 1. Although a full examination of the J-factor uncertainties is beyond the scope of the present work, we note that these uncertainties do not diminish the power of the joint likelihood approach and can be fully accounted for in our analysis procedure by updating the uncertainty parameter in the J-factor likelihood (Equation 3.6).

5   Discussion and Conclusions

This work presents, for the first time, limits on the DM annihilation cross-section from a comprehensive analysis of gamma-ray data with energies between 500 MeV and 10 TeV. Using a common analysis approach (both in the applied statistical methods and in the determination of the J-factors) we have combined the MAGIC observations of Segue 1 with *Fermi*-LAT observations of 15 dSphs. This allowed the computation of meaningful global DM limits, and the direct comparison of the individual results obtained with the different instruments. Our results span the DM particle mass range from 10 GeV to 100 TeV – the widest range covered by a single gamma-ray analysis to date.

We find no signal of DM in our data set. Consequently, we set upper limits to the annihilation cross-section. The obtained results are the most constraining bounds in the considered mass range, from observations of dSphs. For the low-mass range, our results (dominated by *Fermi*-LAT) are below the thermal relic cross-section $\langle \sigma v \rangle \simeq 2.2 \times 10^{-26}$ cm^3 s^{-1}. In the intermediate mass range (from few hundred GeV to few tens TeV, depending on the considered annihilation channel), where *Fermi*-LAT and MAGIC achieve comparable sensitivities, the improvement of the combined result with respect to the individual ones reaches a factor ~ 2. In addition, we present limits to DM particle masses above 10 TeV (dominated by MAGIC) that have not been shown before.

Our global analysis method is completely generic, and can be easily extended to include data from more targets, instruments and/or messenger particles provided they have similar sensitivity to the considered DM particle mass range. Of particular interest is the case of a global DM search from dSphs including data from all current gamma-ray (*Fermi*-LAT, MAGIC, H.E.S.S, VERITAS, HAWC) and neutrino (Antares, IceCube, SuperKamiokande) instruments, and we hereby propose a coordinated effort toward that end. Including results obtained from other types of observational targets like the Galactic Center, galaxy clusters or others is formally also possible, but a common approach to the J-factor determination remains an open question. In the future, this analysis could include new instruments like CTA [58], GAMMA-400 [59], DAMPE [60] or Km3Net [61].[13] Our global approach offers the best chances for indirect DM discovery, or for setting the most stringent limits attainable by these kind of observations.

---

[13]The combination with results from direct searches or accelerator experiments following a similar approach is, in principle, also formally possible, but it would necessarily be model-dependent. This possibility should be however regarded as the culminating step of our proposal.

Acknowledgments

A Comparison with previous MAGIC results

The data, IRFs and likelihood functions (Equations 3.12 to 3.16) used in this work are the same as for previous MAGIC Segue 1 publication [32]. Aside from enlarging the explored DM mass range, the only differences between the two works are: the assumed J-factor central value, the treatment of the J-factor statistical uncertainties, and the prescription used for cases when the maximum of the profile likelihood is found in the non-physical ($\langle \sigma v \rangle < 0$) region. We motivate each of these changes and comment on their effect in the following paragraphs.

- In this work, J-factors are obtained following Ref. [42] and assuming an NFW DM density profile, whereas previous MAGIC results were obtained assuming an Einasto profile [31, 55]. This change has been introduced to homogenize MAGIC and *Fermi*-LAT computation of J-factors, and produces a factor 2 lower (stronger) MAGIC limits with respect to the previously published ones.

- Previous MAGIC results did not include statistical uncertainties in the J-factor. This was justified by the fact that $\langle \sigma v \rangle^{\mathrm{UL}}$ scales with $1/J$, and therefore the provided results allow to compute limits for any J-factor value. This argument is true only for single-target limits, but not for results obtained combining observations from different

targets with different J values and uncertainties. In this study, we include the statistical uncertainties on J for all targets as described in Section 3.2. In consequence, MAGIC limits increase (degrade) by a factor between $\sim$1.4 and $\sim$1.8 (depending on the considered annihilation channel and mass) with respect to the previously published ones.

However, for the scalability argument given before, it is also interesting to provide single-target (Segue 1) results with and without uncertainties on the J-factor, which are shown in Figure 3.

- The requirement of producing upper limits in the physical ($\langle\sigma v\rangle \geq 0$) region normally leads to ad-hoc recipes implying over-coverage (see e.g. Ref. [52]). The problem arises when $\widehat{\langle\sigma v\rangle} < 0$, and it is aggravated when $\langle\sigma v\rangle_{2.71} < 0$. One possible prescription to deal with these cases is to restrict $-2\ln\lambda_P(\langle\sigma v\rangle\,|\,\mathcal{D})$ to $\langle\sigma v\rangle \geq 0$ [56]. This is the solution adopted by $Fermi$-LAT in Refs. [33, 34], and the one we have followed in this work.

  Another, more conservative (i.e. producing larger over-coverage) prescription, was followed by MAGIC in Ref. [32], consisting in computing the 95% confidence limits as $\langle\sigma v\rangle_{\rm svt} = \langle\sigma v\rangle_{2.71} - \widehat{\langle\sigma v\rangle}$, whenever $\widehat{\langle\sigma v\rangle} < 0$. $\langle\sigma v\rangle_{\rm svt}$ corresponds to what the authors in Ref. [57] define as the "sensitivity" of the measurement. Using this prescription, $\langle\sigma v\rangle_{\rm svt}$ is the lowest possible value of the upper limit, irrespective of the presence of arbitrarily intense negative background fluctuations.

  The latter approach cannot be applied to $Fermi$-LAT analysis since, due to low bin statistics, the likelihood function can be undefined for negative $\langle\sigma v\rangle$ values (see Equation 4 in Ref. [34]). We therefore homogenize the treatment of limits close to the physical boundary for our whole data set by limiting $\langle\sigma v\rangle$ to non-negative values. The difference between old and new prescriptions in MAGIC individual limits goes, depending on the annihilation channel and DM particle mass, from none (when $\widehat{\langle\sigma v\rangle} \geq 0$) up to a factor $\sim$4 (for $\sim 2\sigma$ background fluctuations, see Figures 2 and 3).

References

[1] F. Zwicky, *Die Rotverschiebung von extragalaktischen Nebeln*, Helv. Phys. Acta **6** (1933) 110

[2] H. W. Babcock, *The rotation of the Andromeda Nebula*, Lick Observatory Bulletin **19** (1939) 41

[3] P. Salucci and M. Persic, *Dark Halos around Galaxies*, in Dark and visible matter in Galaxies, ASP. Conf. Ser. Vol. 117 (1997) 1. [`arXiv:astro-ph/9703027`]

[4] C. L. Bennett, et al., *First Year Wilkinson Microwave Anisotropy Probe (WMAP) Observations: Preliminary Maps and Basic Results*, Astrophys. J. Suppl. 148 (2003) 1 [`arXiv:astro-ph/0302207`]

[5] P. A. R. Ade et al. *Planck 2015 results. XIII. Cosmological parameters.* [`arXiv:1502.01589`]

[6] P. Hut, *Limits on masses and number of neutral weakly interacting particles*, Phys. Lett. **B69** (1977) 85

[7] G. Gelmini and P. Gondolo, *DM production mechanisms*, in "Particle Dark Matter: Observations, Models and Searches", G. Bertone (Editor). Cambridge U. Press, Cambridge 2010, Chap.7, p.121. [`arXiv:1009.3690`]

[8] F. Aharonian et al., *H.E.S.S. observations of the Galactic Center region and their possible dark matter interpretation* , Phys. Rev. Lett. **97** (2006) 221102. [`arXiv:astro-ph/0610509`]

[9] J. Albert et al., *Observation of Gamma Rays from the Galactic Center with the MAGIC telescope*, Astrophys. J. **638** (2006) L101. [arXiv:astro-ph/0512469]

[10] A. Archer et al., *Very-High Energy Observations of the Galactic Center Region by VERITAS in 2010-2012*, Astrophys. J. **790** (2014) 149. [arXiv:1406.6383]

[11] A. Abramowski et al., *Search for a Dark Matter annihilation signal from the Galactic Center halo with H.E.S.S.* . Phys. Rev. Lett. **106** (2011) 161301. [arXiv:1103.3266]

[12] M. Ackermann et al. *Constraints on the Galactic Halo Dark Matter from Fermi-LAT Diffuse Measurements*, Astrophys. J. **761** (2012) 91. [arXiv:1205.6474]

[13] A. Abramowski et al., *Search for photon line-like signatures from Dark Matter annihilations with H.E.S.S*, Phys. Rev. Lett. **110** (2013) 041301. [arXiv:1301.1173]

[14] M. Ackermann et al. *Search for gamma-ray spectral lines with the Fermi Large Area Telescope and dark matter implications*, Phys. Rev. **D88** (2013) 082002. [arXiv:1305.5597]

[15] A. U. Abeysekara et al., *The Sensitivity of HAWC to High-Mass Dark Matter Annihilations*, Phys. Rev. **D90** (2014) 122002. [arXiv:1405.1730]

[16] R. Abbasi et al. *Search for Dark Matter from the Galactic Halo with the IceCube Neutrino Telescope*, Phys. Rev. **D84** (2011) 022004. [arXiv:1101.3349]

[17] S. Adrián-Martínez, *Search of Dark Matter Annihilation in the Galactic Centre using the ANTARES Neutrino Telescope.* [arXiv:1505.04866]

[18] J. Aleksić et al., *MAGIC Gamma-Ray Observation of the Perseus Galaxy Cluster*, Astrophys. J. **710** (2010) 634. [arXiv:0909.3267]

[19] A. Abramowski et al., *Erratum to "Search for Dark Matter Annihilation Signals from the Fornax Galaxy Cluster with H.E.S.S"*, Astrophys. J. **783** (2014) 63

[20] T. Arlen et al., *Constraints on Cosmic Rays, Magnetic Fields, and Dark Matter from Gamma-Ray Observations of the Coma Cluster of Galaxies with VERITAS and Fermi*, Astrophys. J. **757** (2012) 123. [arXiv:1208.0676]

[21] M. Ackermann et al. *Constraints on Dark Matter Annihilation in Clusters of Galaxies with the Fermi Large Area Telescope*, JCAP **05** (2010) 025. [arXiv:1002.2239]

[22] M. G. Aartsen et al. *An IceCube Search for Dark Matter Annihilation in Nearby Galaxies and Galaxy Clusters*, Phys. Rev. **D88** (2013) 122001. [arXiv:1307.3473]

[23] F. Aharonian et al., *Erratum to "Observations of the Sagittarius Dwarf galaxy by the H.E.S.S. experiment and search for a Dark Matter signal"*, Astropart. Phys. **33** (2010) 274

[24] F. Aharonian et al., *A search for a dark matter annihilation signal towards the Canis Major overdensity with H.E.S.S*, Astrophy. J. **691** (2009) 175. [arXiv:0809.3894]

[25] A. Abramowski et al., *H.E.S.S. constraints on Dark Matter annihilations towards the Sculptor and Carina Dwarf Galaxies*, Astropart. Phys. **34** (2011) 608. [arXiv:1012.5602]

[26] A. Abramowski et al., *Search for dark matter annihilation signatures in H.E.S.S. observations of Dwarf Spheroidal Galaxies*, Phys. Rev. D in press (2015). [arXiv:1410.2589]

[27] V. A. Acciari et al., *VERITAS Search for VHE Gamma-ray Emission from Dwarf Spheroidal Galaxies.* Astrophys. J. **720** (2010) 1174. [arXiv:1006.5955]

[28] E. Aliu et al., *Erratum to "VERITAS deep observations of the dwarf spheroidal galaxy Segue 1".* Phys. Rev. **D91** (2015) 129903(E)

[29] J. Albert et al., *Upper limit for gamma-ray emission above 140 GeV from the dwarf spheroidal galaxy Draco.* Astrophys. J. **679** (2008) 428. [arXiv:0711.2574]

[30] J. Albert et al., *Upper Limits on the VHE Gamma-Ray Emission from the Willman 1 Satellite Galaxy with the Magic Telescope.* Astrophys. J. **697** (2009) 1299. [arXiv:0810.3561]

[31] J. Aleksić et al., *Searches for dark matter annihilation signatures in the Segue 1 satellite galaxy with the MAGIC-I telescope*, JCAP **06** (2011) 035. [arXiv:1103.0477]

[32] J. Aleksić et al., *Optimized dark matter searches in deep observations of Segue 1 with MAGIC*, JCAP **02** (2014) 008. [arXiv:1312.1535]

[33] M. Ackermann et al., *Dark Matter Constraints from Observations of 25 Milky Way Satellite Galaxies with the Fermi Large Area Telescope*, Phys. Rev. **D89** (2014) 042001. [arXiv:1310.0828]

[34] M. Ackermann et al., *Searching for Dark Matter Annihilation from Milky Way Dwarf Spheroidal Galaxies with Six Years of Fermi-LAT Data.* [arXiv:1503.02641]

[35] M. Ackermann el al. *Limits on Dark Matter Annihilation Signals from the Fermi LAT 4-year Measurement of the Isotropic Gamma-Ray Background.* [arXiv:1501.05464]

[36] M. Ackermann et al. *Search for Dark Matter Satellites using Fermi-LAT*, Astrophys. J. **747** (2012) 121. [arXiv:1201.2691]

[37] M. G. Aartsen et al. *Search for Dark Matter Annihilations in the Sun with the 79-string IceCube Detector* Phys. Rev. Lett. **110** (2013) 131302. [arXiv:1212.4097]

[38] J. Aleksić, J. Rico and M. Martinez, *Optimized analysis method for indirect dark matter searches with Imaging Air Cherenkov Telescopes*, JCAP **10** (2012) 032. [arXiv:1209.5589]

[39] V. Springel et al., *The Aquarius Project: the subhaloes of galactic haloes*, Mon. Not. Roy. Astron. Soc. **391** (2008) 1685. [arXiv:0809.0898]

[40] J. Diemand et al., *Clumps and streams in the local dark matter distribution*, Nature, **454** (2008) 735. [arXiv:0805.1244]

[41] L. E. Strigari, *Galactic searches for dark matter*, Phys. Rep. **531** (2013) 1. [arXiv:1211.7090]

[42] G. D. Martinez, *A Robust Determination of Milky Way Satellite Properties using Hierarchical Mass Modeling.* Mon. Not. Roy. Astron. Soc. **451** (2015) 2524. [arXiv:1309.2641]

[43] A. Geringer-Sameth, S. M. Koushiappas and M. Walker, *Dwarf galaxy annihilation and decay emission profiles for dark matter experiments*, Astrophys. J. **801** (2015) 74. [arXiv:1408.0002]

[44] V. Bonnivard et al. *Dark matter annihilation and decay in dwarf spheroidal galaxies: The classical and ultrafaint dSphs.* Mon. Not. Roy. Astron. Soc. **453** (2015) 849. [arXiv:1504.02048]

[45] J. Aleksić et al., *The major upgrade of the MAGIC telescopes, Part II: The achieved physics performance using the Crab Nebula observations*, Astropart. Phys. **72** (2016) 76. [arXiv:1409.5594]

[46] J. Aleksić et al., *The major upgrade of the MAGIC telescopes, Part I: The hardware improvements and the commissioning of the system*, Astropart. Phys. **72** (2016) 61. [arXiv:1409.6073]

[47] W. B. Atwood et al., *The Large Area Telescope on the Fermi Gamma-ray Space Telescope Mission*, Astrophys. J. **697** (2009) 1071. [arXiv:0902.1089]

[48] M. Ackermann *et al.* [Fermi-LAT Collaboration], *The Fermi Large Area Telescope On Orbit: Event Classification, Instrument Response Functions, and Calibration*, Astrophys. J. Suppl. **203**, 4 (2012). [arXiv:1206.1896]

[49] F. Acero et al., *Fermi Large Area Telescope Third Source Catalog*, Astrophys. J. Suppl. **218**, 23 (2015). [arXiv:1501.02003]

[50] T. Sjöstrand et al. *An Introduction to PYTHIA 8.2*, Comput. Phys. Commun. **191** (2015) 159. [arXiv:1410.3012]

[51] J. F. Navarro, C. S. Frenk, and S. D. White, *A Universal Density Profile from Hierarchical Clustering*, Astrophys. J. **490** (1997) 493. [arXiv:astro-ph/9611107]

[52] K. A. Olive et al. *The Review of Particle Physics*, Chin. Phys. **C38** (2014) 090001

[53] J. Aleksić, *Optimized Dark Matter Searches in Deep Observations of Segue 1 with MAGIC*. Springer Theses (2016). DOI:10.1007/978-3-319-23123-5

[54] G. Steigman, B. Dasgupta and J. F. Beacom, *Precise relic WIMP abundance and its impact on searches for dark matter annihilation* Phys. Rev. **D86** (2012) 023506. [arXiv:1204.3622]

[55] R. Essig et al., *Indirect Dark Matter Detection Limits from the Ultra-Faint Milky Way Satellite Segue 1*, Phys. Rev. **D82** (2010) 123503. [arXiv:1007.4199]

[56] W. A. Rolke, A. M. López, and J. Conrad *Limits and confidence intervals in the presence of nuisance parameters*, Nucl. Instrum. Meth. **A551** (2005) 493. [arXiv:physics/0403059]

[57] G. J. Feldman and R. D. Cousins, *A Unified Approach to the Classical Statistical Analysis of Small Signals*, Phys. Rev. **D57** (1998) 3873. [arXiv:physics/9711021]

[58] M. Doro et al. *Dark Matter and Fundamental Physics with the Cherenkov Telescope Array*, Astropart. Phys. **43** (2013) 189. [arXiv:1208.5356]

[59] A. A. Moiseev et al. *Dark Matter Search Perspectives with GAMMA-400*, in Proc. of the 33rd International Cosmic-Ray Conference 2013, Brazil, Rio de Janeiro. [arXiv:1307.2345]

[60] Y. Dong et al. *DAMPE silicon tracker on-board data compression algorithm*. [arXiv:1503.00415]

[61] B. Dasgupta and R. Laha, *Neutrinos in IceCube/KM3NeT as probes of Dark Matter Substructures in Galaxy Clusters*, Phys. Rev. **D86** (2012) 093001. [arXiv:1206.1322]